Hard and superconducting cubic boron phase via swarm-intelligence structural prediction driven by a machine-learning potential

Qiuping Yang,[1,2,*] Jian Lv,[3,*] Qunchao Tong,[3,*] Xin Du,[1,2] Yanchao Wang,[3] Shoutao Zhang,[1] Guochun Yang,[1,2,†] Aitor Bergara,[4,5,6,‡] and Yanming Ma[3,§]

[1]*Centre for Advanced Optoelectronic Functional Materials Research and Key Laboratory for UV Light-Emitting Materials and Technology of Ministry of Education, Northeast Normal University, Changchun 130024, China*

[2]*State Key Laboratory of Metastable Materials Science & Technology and Key Laboratory for Microstructural Material Physics of Hebei Province, School of Science, Yanshan University, Qinhuangdao 066004, China*

[3]*International Center of Computational Method and Software, State Key Laboratory of Superhard Materials, College of Physics, Jilin University, Changchun 130012, China*

[4]*Departamento de Física de la Materia Condensada, Universidad del País Vasco-Euskal Herriko Unibertsitatea, UPV/EHU, 48080 Bilbao, Spain*

[5]*Donostia International Physics Center (DIPC), 20018 Donostia, Spain*

[6]*Centro de Física de Materiales CFM, Centro Mixto CSIC-UPV/EHU, 20018 Donostia, Spain*

(Received 14 October 2020; revised 26 November 2020; accepted 16 December 2020; published 8 January 2021)

Boron is an intriguing element due to its electron deficiency and the ability to form multicenter bonds in allotropes and borides, exhibiting diversified structures, unique chemical bonds, and interesting properties. Using swarm-intelligence structural prediction driven by a machine learning potential, we identified a boron phase with a 24-atom cubic unit cell, called c-B_{24}, consisting of a B_6 octahedron in addition to well-known B_2 pairs and B_{12} icosahedra at ambient pressure. There appear unusual four-center-two-electron (4c-2e) bonds in the B_{12} icosahedron, originating from the peculiar bonding pattern between the B_2 pair and B_{12} icosahedron, which is in sharp contrast with the 3c-2e and 2c-2e bonds in α-B_{12}. More interestingly, c-B_{24} is a metal with a superconducting critical temperature of 13.8 K at ambient pressure. The predicted Vickers hardness (23.1 GPa) indicates that c-B_{24} is a potential hard material. Notably, it also has a good shear/tensile resistance (48.9/29.3 GPa). Our work not only enriches the understanding of the chemical properties of boron, but also sparks efforts on trying to synthesize this particular compound, c-B_{24}.

DOI: 10.1103/PhysRevB.103.024505

I. INTRODUCTION

Allotropes, which refer to different forms of the same element, have become a fascinating area of research in condensed matter physics and chemistry [1–3]. Finding new allotropes, with unique structural units and a combination of several chemical bonds, allows a deeper understanding of the chemical behavior of the elements [4–6]. On the other hand, the preparation of allotropes is an important way to obtain functional materials with fascinating properties [7–10]. A large number of allotropes are already known, especially for the light elements, as carbon, silicon, nitrogen, and boron, but there are still interesting surprises to be discovered [11–17]. This is basically due to their complex potential energy surfaces with a plethora of local minima, which causes diversified metastable structures (i.e., allotropes) to exist [18–22]. For example, in addition to the five known nitrogen allotropes [23], an allotrope with the black phosphorus structure has been found very recently [24,25].

Boron has three valence electrons and, following the classical valence bond theory, it can only form three covalent bonds with three boron/other atoms forming allotropes or compounds. However, its ability to form multicenter bonds greatly enriches its structural diversity [26]. So far, at least 16 boron allotropes have been reported [14], with various electronic properties (e.g., semiconductivity, metallicity, semimetallicity, and superconductivity). On the other hand, the properties of boron allotropes are strongly correlated with binding patterns and the arrangement of structural units [14,21,27]. Specifically, *Pnma*-B_{60}, where B_{12} icosahedra are linked by two-atom wide boron ribbons, is a semimetal, whereas $I2_12_12_1$-B_{60}, in which B_{12} icosahedra are interconnected by helical boron chains, is a metal [28]. Taking into account the complex potential energy surfaces and diversified binding patterns of boron [29,30], which favors the formation of novel structural units or different combinations of already known structural units, it is still possible to find new boron allotropes.

Recently, theoretical prediction plays a critical and leading role in accelerating the discovery of new allotropes [22,31–34]. In this work, we employ the swarm-intelligence structural search method combined with a machine learning potential to search for new boron allotropes at ambient pressure containing up to 60 B atoms. In addition to

*These authors contributed equally to this work.
†Corresponding author: yanggc468@nenu.edu.cn
‡Corresponding author: a.bergara@ehu.eus
§Corresponding author: mym@jlu.edu.cn

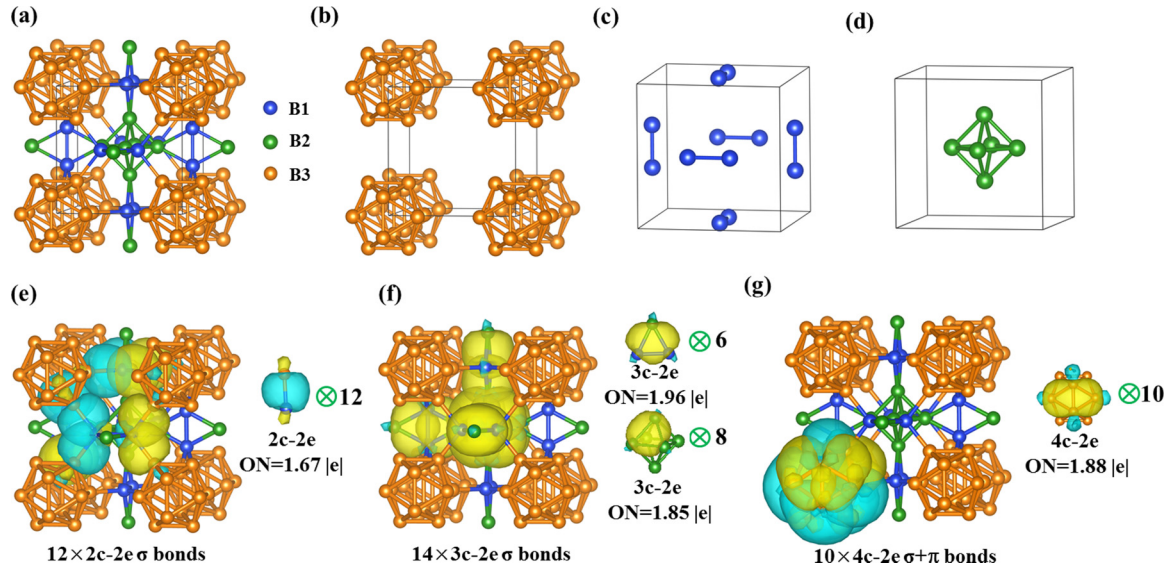

FIG. 1. (a) Crystal structure of the c-B_{24} phase. The location of the (b) B_{12} icosahedra, (c) B_2 pairs, and (d) B_6 octahedra in the lattice. The SSAdNDP chemical bonding analysis of c-B_{24} along with the occupation number (ON). In total 36 bonds are showed, including (e) 12 2c-2e σ bonds, (f) 14 3c-2e σ bonds, and (g) 10 4c-2e $\sigma+\pi$ bonds. The "+" symbol represents an overlap between the σ and π bonds.

replicating the four reported boron allotropes (e.g., α-B_{12} [35], γ-B_{28} [14], α-Ga-type B [36], and B_{10} [37]), we have found one, named c-B_{24}, which shows a different structural unit (B_6 octahedron) situated at the center of the cubic unit cell. On the other hand, the unique arrangement between B_{12} icosahedron and the B_2 pair induces a 4c-2e bond in the B_{12} icosahedron. More interestingly, c-B_{24} is both hard and superconducting.

II. COMPUTATIONAL DETAILS

The crystal structure search is performed with the swarm-intelligence CALYPSO method [38–40] driven by a modified version of the Gaussian approximation potential (GAP) [41]. Compared with the original GAP [42], the atomic-centered symmetry function [43], rather than the smooth overlap of atomic positions [44], was used as descriptors to describe neighboring environment of B atoms. The CALYPSO method has been successfully applied in many systems, including C_{84} clusters, [41] C_{10} [45], TiO_2 [46], and some organic materials [47]. In this work, the already known four stable boron phases (α-B_{12}, γ-B_{28}, α-Ga-type B, and B_{10}) are successfully replicated [14,37,48–52], demonstrating the reliability of the method in the global structure search. More detailed information can be found in the Supplemental Material [53].

The underlying structural relaxation and electronic properties are carried out by employing the Vienna *ab initio* simulation package (VASP) [54,55]. The electron-ion interaction is represented by the full electron projection augmented wave method [56], and $2s^2 2p^1$ are treated as valence electrons of B. The plane wave basis with a kinetic energy cutoff of 800 eV is used, and a Monkhorst-Pack scheme [57] with a dense k-point grid spacing of $2\pi \times 0.03$ Å^{-1} is chosen to ensure a good convergence of the total energy. Phonon calculations are performed by using the finite displacement approach [58] in the PHONOPY code [59]. First-principles molecular dynamics simulations [60] using the canonical *NVT* are performed with a time step of 1 fs to evaluate the thermal stability of the predicted structures. Electron-phonon coupling (EPC) calculations were performed with density functional perturbation theory using the Quantum-ESPRESSO package [61].

III. RESULTS AND DISCUSSION

A. Structure, chemical bonding, and stability

After an extensive structural search at ambient pressure, we found a cubic structure with the space group $Pm\bar{3}$, containing 24 atoms in the unit cell, named c-B_{24} [Fig. 1(a)]. Within this structure, three inequivalent B atoms occupy the crystallographic 6g (0.3528, 0.5000, 0.0000), 6h (0.7204, 0.5000, 0.5000), and 12j (0.0000, 0.8414, 0.2540) sites, which form three kinds of structural units, i.e., B_6 octahedron, B_2 pair, and B_{12} icosahedron, Figs. 1(b)–1(d), located at the body center, face center, and vertex of the cubic lattice, respectively. The B atoms in B_2 units are connected with the vertex B atoms in the B_{12} icosahedra and the B_6 octahedron to form a dense three-dimensional packing structure. Notably, B_6 octahedron appears in the reported boron allotropes, but it has also been observed in metal borides at ambient (e.g., BeB_6, MgB_6, CaB_6, LaB_6, and YB_6) [62–64] and high pressures (e.g., BaB_6 and KB_6) [65,66].

It is well-known that B atoms tend to form multicenter bonds, playing a key role in stabilizing allotropes and B-rich borides [26,67]. Furthermore, the presence of B_6 octahedra and the unique bonds between B_2 structural units and B_{12} icosahedra lead us to explore the characteristics of these chemical bonds. Here, the solid state adaptive natural density partitioning (SSAdNDP) method [68], whose efficacy has been verified in a plethora of compounds [69,70], is used to study the binding patterns in c-B_{24}. The unit cell of c-B_{24}, with 72 valence electrons, presents 12 2c-2e bonds at the junction between B_{12} icosahedra and B_2 pairs [Fig. 1(e)], eight 3c-2e bonds in B_6 octahedra, and six 3c-2e bonds at the intersection between B_6 octahedra and B_2 pairs [Fig. 1(f)]. More

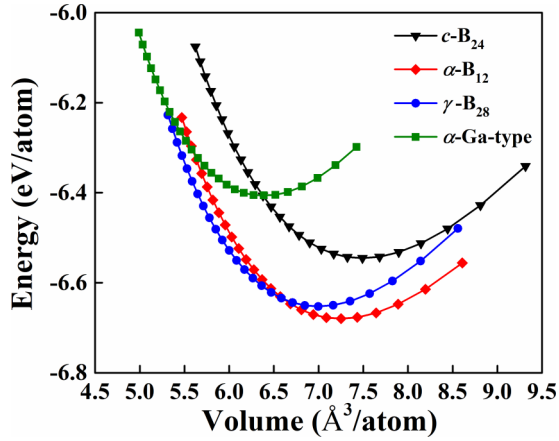

FIG. 2. Total energy of c-B_{24} as a function of the volume per atom in comparison with those of α-B_{12}, γ-B_{28}, and α-Ga-type boron.

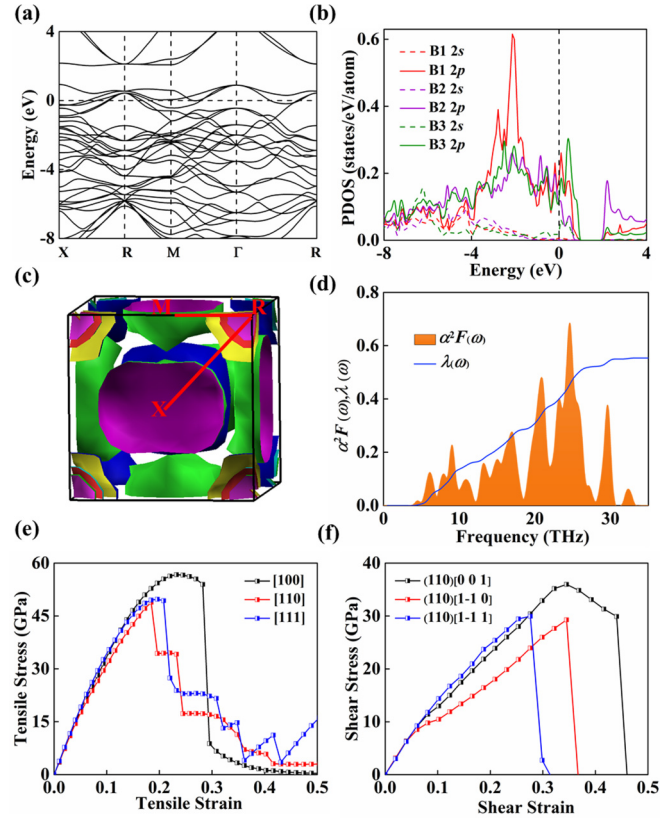

FIG. 3. (a) The electronic band structure of c-B_{24} at 1 atm. (b) Projected density of states (PDOS) of c-B_{24} with different occupying sites at 1 atm. (c) The Fermi surface for c-B_{24} at 1 atm. (Fig. S5 shows the Fermi surface associated with each band crossing the Fermi level.) (d) The Eliashberg spectral function $\alpha^2F(\omega)$ and integrated electron-phonon coupling parameters $\lambda(\omega)$ of c-B_{24} at 1 atm. (e) The calculated stress-strain relations of phase c-B_{24} in the three stress tension directions. (f) The calculated stress-shear for c-B_{24} in the three principal symmetry crystallographic directions.

interestingly still, 10 4c-2e bonds appear in the B_{12} icosahedral unit [Fig. 1(g)], which is in sharp contrast with the B_{12} icosahedron in α-B_{12} (i.e., with strong 2c-2e and weak 3c-2e bonds) [14,71]. This could be attributed to their different atomic arrangements. Specifically, in c-B_{24} every boron atom in the icosahedral unit B_{12} is bonded to B atoms in B_2 units, forming 12 B–B bonds (Fig. S2). In α-B_{12}, the icosahedral units connect each other with six pairs of B–B bonds. The 4c-2e bonds have been observed in two-dimensional (2D) materials, such as the α-boron sheet [69], and have also been reported in boron triangle units of bulk α' boron [72], whose atomic arrangement is completely different from the B_{12} icosahedron. The unique bonding combination might induce different electronic properties. In addition, the average B−B bond length in c-B_{24} is 1.77 Å, which is equal and slightly shorter than 1.77 Å in α-B_{12} and 1.82 Å in γ-B_{28}. The average Mulliken overlap population of c-B_{24} (0.63) is slightly larger than that of α-B_{12} (0.56) and γ-B_{28} (0.55), indicating that B–B bonds in c-B_{24} are stronger.

The thermodynamic stability of the predicted structure can be used to evaluate the feasibility of the experimental synthesis. Figure 2 shows the calculated total energy versus volume of c-B_{24}, compared to the three already reported boron allotropes (e.g., α-B_{12} [35], γ-B_{28} [14], and α-Ga-type B [36]). At ambient conditions, it can be clearly seen that α-B_{12} has the lowest value of the total energy per atom, and α-Ga-type boron shows the maximum one, which is consistent with previous reports [14] and supports the reliability of our calculations. At ambient pressure, c-B_{24} is 0.139 eV/atom lower in energy than α-Ga-type boron, but 0.134 and 0.107 eV/atom higher in energy than α-B_{12} and γ-B_{28}, respectively. Several metastable phases have been synthesized with much higher energy than the most stable phase, such as M-carbon (0.283 eV/atom higher than graphite) [12], the nitrogen allotrope with black phosphorus structure (1.12 eV/atom higher than α-N) [24], and the Si-III structure (0.16 eV/atom higher than Si-I) [73]. These results imply that c-B_{24} could be synthesized in certain conditions and exist as a metastable phase.

Phonon dispersions of c-B_{24} without any imaginary frequency in the whole Brillouin zone demonstrate that it is dynamically stable at both ambient (Fig. S3) and high pressures (i.e., 25 and 50 GPa, Fig. S3). To examine the thermal stability, *ab initio* molecular dynamics simulations are also performed with the canonical (*NVT*) ensemble at 1000 K, using the Nosé thermostat [60] with a step of 1 fs. We model the system using a $2 \times 2 \times 2$ supercell that has 192 B atoms. Energy fluctuations at 1000 K are shown in Fig. S4, and the initial and final structures are also presented. Interestingly, the framework of c-B_{24} maintains its original configuration at 1000 K, exhibiting an outstanding thermal stability. Furthermore, c-B_{24} satisfies the criteria for mechanical stability, as will be discussed later.

B. Electronic properties and superconducting

The appearance of different B_6 octahedra and unique 4c-2e bonds in the B_{12} icosahedra stimulate us to explore its electronic properties. The calculated electronic band structure and the corresponding projected density of states (PDOS) at the Perdew-Burke-Ernzerhof (PBE) level are shown in Figs. 3(a) and 3(b). Unexpectedly, c-B_{24} is a metal with several bands crossing the Fermi level, which is in sharp contrast with the nonmetallic α-B_{12} [14] and γ-B_{28} [14] but similar to the

α-Ga-type boron [36] at ambient pressure. PDOS analysis shows that its metallicity comes mainly from the contribution of B $2p$. On the other hand, there is a strong overlap between B $2p$ in B_2 units and B $2p$ in B_6 octahedra and B_{12} icosahedra, indicating the formation of strong chemical bonds, in line with the previous chemical bond analysis. The contribution of B $2s$ in B_{12} icosahedra to metallicity is much higher than that of the B_2 units and B_6 octahedra, which could originate from the unique 4c-2e bonds in the B_{12} icosahedra. In addition, a well-defined Fermi surface nesting appears along X→R and R→M [Fig. 3(c)], with highly dispersive bands in the two directions. On the contrary, flatter bands associated with more localized electronic states appear along X→R, which induces a high electronic density of states near the Fermi level.

Motivated by the strong PDOS peak at the Fermi level and the presence of steep bands along the Γ→M direction and flat bands along the X→R direction, we have explored the superconductivity of c-B_{24}. The superconducting transition temperature (T_c) was estimated by using the Allen and Dynes modified McMillan equation with a typical choice of $\mu^* = 0.1$ [74–77]. The calculated T_c of c-B_{24} is 13.8 K at ambient pressure, becoming the first superconductor among known bulk boron allotropes at 0 GPa, and is much higher than 6 K of β-B at 175 GPa [78] and comparable to 2D B polymorphs (e.g., 18.7 K for β_{12}, [79] 24.7 K for χ^3 [79], and 17.9 K for 2D boron layer [66]).

The integrated electron-phonon coupling parameter λ (ω) and Eliashberg spectral function $\alpha^2F(\omega)$ are shown in Fig. 3(d). The calculated λ is 0.55, which is higher than 0.38, 0.39, and 0.39 at 160, 215, 273 GPa of α-Ga-type boron [80], 0.39 for the boron-doped diamond with 2.78% boron content [81] and comparable to 0.61 in MgB_2 [82]. The contribution of low-, mid-, and high-frequency modes to the EPC are 29.5% (below 12 THz), 22% (12 ∼ 19 THz), and 48.4% (above 19 THz), respectively. Therefore, its superconducting mechanism is different from the low-frequency P-derived vibrations of the Li_6P electride [83], high-frequency H-derived vibrations of high-T_c H_3S [84], and intermediate-frequency H-derived vibrations of H_4Te [85]. We also explored its pressure dependence T_c. As shown in Fig. S6, the T_c of c-B_{24} increases with pressure (e.g., 14.6 K at 25 and 17.1 K at 50 GPa), which mainly originates from the pressure-induced phonon softening along X→R in the Brillouin zone (Fig. S3), leading to an enhancement of λ.

C. Mechanical property and hardness

The calculated bulk modulus (B), shear modulus (G), Young's modulus (E), and Poisson's ratio (ν) of c-B_{24} are given in Table S3. Overall, B is a measure of the tensile strength of the material. The higher B is, the more incompressible it is. The bulk modulus (B) of c-B_{24} is 209.38 GPa, which is comparable to other known hard materials [e.g., Al_2O_3 (254 GPa) and AlN (205 GPa)] [86,87].The ratio between the bulk modulus and the shear modulus (B/G) is used to measure the brittle or ductile behavior of materials [88]. The calculated B/G of c-B_{24} is 1.373, which is much lower than the criterion value (1.75) for considering a material to be ductile. In addition, Poisson's ratio (ν) provides a useful information about the characteristics of the bonding forces. The resulting Poisson's ratio of c-B_{24} is 0.207, which shows a large lateral expansion when it is compressed [89]. Finally, the calculated Vickers hardness value of c-B_{24} is 23.1 GPa, which is less than that of the recent superhard boron, orthorhombic γ-B_{28} (50 GPa) [90]. It is comparable to some typical hard materials [87] [e.g., WC (30 GPa), TiN (23 GPa), ZrC (25.8 GPa), and TiC (24.7 GPa)]. Moreover, stress-strain relations can reflect the ability of a material to resist shear and tension. The calculated tensile stress-strain relations of c-B_{24} in the three principal symmetry crystallographic directions ([001], [110], and [111]) are presented in Fig. 3(e). When the critical tensile stain (ε) is above 0.18, the B–B bonds between B_2 units and B_{12} icosahedra are broken (Fig. S7) along the [110] direction, corresponding to a peak stress of 48.9 GPa. Tensile stress along the [001] direction has the lowest peak value in the (110) plane [Fig. 3(f)] and the shear direction [1–10] shows a peak value of 29.3 GPa.

IV. CONCLUSIONS

In search of possible boron allotropes, we explored configurations that have up to 60 atoms with the help of swarm-intelligence structural search in combination with the state-of-art machine learning potential at ambient pressure. A hitherto unknown pristine 3D crystalline boron, c-B_{24}, is identified, that exhibits high dynamical, mechanical, and thermal stability, as well as an alternative chemical bonding pattern (i.e., 4c-2e bond) in the B_{12} icosahedron. Interestingly, c-B_{24} shows superconductivity with a T_c value of 13.8 K at ambient pressure; additionally, considering its predicted Vickers hardness of 23.1 GPa, as well as its good tensile and shear strengths of 48.9 and 29.3 GPa, respectively. Our work should help to expand the members of the boron family, and promote further investigations on different boron allotropes with desirable electronic and mechanical properties.

ACKNOWLEDGMENTS

The authors acknowledge the funding support from the Natural Science Foundation of China under Grants No. 21873017, No. 21573037, No. 11704062, and No. 51732003, the Postdoctoral Science Foundation of China under Grant No. 2013M541283, the Natural Science Foundation of Jilin Province (20190201231JC), the "111" Project (No. B13013). The work was carried out at National Supercomputer Center in Tianjin, and the calculations were performed on TianHe-1 (A). A.B. acknowledges financial support from the Spanish Ministry of Science and Innovation (PID2019-105488GB-I00) and from Jilin Province Out-standing Young Talents project (Grant No. 20190103040JH).

[1] W. B. Jensen, J. Chem. Educ. **83**, 838 (2006).
[2] A. Hirsch, Nat. Mater. **9**, 868 (2010).
[3] V. Georgakilas, J. A. Perman, J. Tucek, and R. Zboril, Chem. Rev. **115**, 4744 (2015).

[4] S. Zhang, J. Zhou, Q. Wang, X. Chen, Y. Kawazoe, and P. Jena, Proc. Natl. Acad. Sci. USA **112**, 2372 (2015).

[5] Q. Wang, B. Xu, J. Sun, H. Liu, Z. Zhao, D. Yu, C. Fan, and J. He, J. Am. Chem. Soc. **136**, 9826 (2014).

[6] K. Umemoto, R. M. Wentzcovitch, S. Saito, and T. Miyake, Phys. Rev. Lett. **104**, 125504 (2010).

[7] F. Diederich and Y. Rubin, Angew Chem. Int. Ed. English **31**, 1101 (1992).

[8] M. I. Eremets, A. G. Gavriliuk, I. A. Trojan, D. A. Dzivenko, and R. Boehler, Nat. Mater. **3**, 558 (2004).

[9] D. Tomasino, M. Kim, J. Smith, and C.-S. Yoo, Phys. Rev. Lett. **113**, 205502 (2014).

[10] D. Laniel, G. Geneste, G. Weck, M. Mezouar, and P. Loubeyre, Phys. Rev. Lett. **122**, 066001 (2019).

[11] T. Irifune, A. Kurio, S. Sakamoto, T. Inoue, and H. Sumiya, Nature (London) **421**, 599 (2003).

[12] Q. Li, Y. Ma, A. R. Oganov, H. Wang, H. Wang, Y. Xu, T. Cui, H.-K. Mao, and G. Zou, Phys. Rev. Lett. **102**, 175506 (2009).

[13] Z. Zhao, B. Xu, X.-F. Zhou, L.-M. Wang, B. Wen, J. He, Z. Liu, H.-T. Wang, and Y. Tian, Phys. Rev. Lett. **107**, 215502 (2011).

[14] A. R. Oganov, J. Chen, C. Gatti, Y. Ma, Y. Ma, C. W. Glass, Z. Liu, T. Yu, O. O. Kurakevych, and V. L. Solozhenko, Nature (London) **457**, 863 (2009).

[15] W. D. Mattson, D. Sanchez-Portal, S. Chiesa, and R. M. Martin, Phys. Rev. Lett. **93**, 125501 (2004).

[16] B. Hirshberg, R. B. Gerber, and A. I. Krylov, Nat. Chem. **6**, 52 (2014).

[17] X. Wu, X. Shi, M. Yao, S. Liu, X. Yang, L. Zhu, T. Cui, and B. Liu, Carbon **123**, 311 (2017).

[18] B. D. Malone and M. L. Cohen, Phys. Rev. B **85**, 024116 (2012).

[19] M. Xing, B. Li, Z. Yu, and Q. Chen, Materials **9**, 484 (2016).

[20] D. Fan, S. Lu, A. A. Golov, A. A. Kabanov, and X. Hu, J. Chem. Phys. **149**, 114702 (2018).

[21] C. Fan, J. Li, and L. Wang, Sci. Rep. **4**, 6786 (2014).

[22] D. Li, F. Tian, B. Chu, D. Duan, S. Wei, Y. Lv, H. Zhang, L. Wang, N. Lu, B. Liu, and T. Cui, J. Mater. Chem. A **3**, 10448 (2015).

[23] L. Lei, Q.-Q. Tang, F. Zhang, S. Liu, B.-B. Wu, and C.-Y. Zhou, Chin. Phys. Lett. **37**, 068101 (2020).

[24] C. Ji, C. Ji, A. A. Adeleke, L. Yang, B. Wan, H. Gou, Y. Yao, B. Li, Y. Meng, J. S. Smith, V. B. Prakapenka, W. Liu, G. Shen, W. L. Mao, and H. K. Mao, Sci. Adv. **6**, eaba9206 (2020).

[25] D. Laniel, B. Winkler, T. Fedotenko, A. Pakhomova, S. Chariton, V. Milman, V. Prakapenka, L. Dubrovinsky, and N. Dubrovinskaia, Phys. Rev. Lett. **124**, 216001 (2020).

[26] H. Zhang, Y. Li, J. Hou, K. Tu, and Z. Chen, J. Am. Chem. Soc. **138**, 5644 (2016).

[27] K. Shirai, Jpn. J. Appl. Phys. **56**, 05FA06 (2017).

[28] X.-L. He, X. Shao, T. Chen, Y.-K. Tai, X.-J. Weng, Q. Chen, X. Dong, G. Gao, J. Sun, X.-F. Zhou, Y. Tian, and H.-T. Wang, Phys. Rev. B **99**, 184111 (2019).

[29] V. L. Deringer, C. J. Pickard, and G. Csányi, Phys. Rev. Lett. **120**, 156001 (2018).

[30] E. V. Podryabinkin, E. V. Tikhonov, A. V. Shapeev, and A. R. Oganov, Phys. Rev. B **99**, 064114 (2019).

[31] J. Zhang, R. Wang, X. Zhu, A. Pan, C. Han, X. Li, D. Zhao, C. Ma, W. Wang, H. Su, and C. Niu, Nat. Commun. **8**, 683 (2017).

[32] S. Liu, L. Zhao, M. Yao, M. Miao, and B. Liu, Adv. Sci. **7**, 1902320 (2020).

[33] J. Kotakoski and K. Albe, Phys. Rev. B **77**, 144109 (2008).

[34] Q. Fan, H. Wang, Y. Song, W. Zhang, and S. Yun, Comput. Mater. Sci. **178**, 109634 (2020).

[35] A. R. Oganov and V. L. Solozhenko, J. Superhard. Mater. **31**, 285 (2009).

[36] U. Häussermann, S. I. Simak, R. Ahuja, and B. Johansson, Phys. Rev. Lett. **90**, 065701 (2003).

[37] D. Li, K. Bao, F. Tian, X. Jin, D. Duan, Z. He, B. Liu, and T. Cui, RSC Adv. **4**, 203 (2014).

[38] Y. Wang, J. Lv, L. Zhu, and Y. Ma, Phys. Rev. B **82**, 094116 (2010).

[39] Y. Wang, J. Lv, L. Zhu, and Y. Ma, Comput. Phys. Commun. **183**, 2063 (2012).

[40] B. Gao, P. Gao, S. Lu, J. Lv, Y. Wang, and Y. Ma, Sci. Bull. **64**, 301 (2019).

[41] Q. Tong, L. Xue, J. Lv, Y. Wang, and Y. Ma, Faraday Discuss **211**, 31 (2018).

[42] A. P. Bartók, M. C. Payne, R. Kondor, and G. Csányi, Phys. Rev. Lett. **104**, 136403 (2010).

[43] J. Behler, J. Chem. Phys. **134**, 074106 (2011).

[44] A. P. Bartók, R. Kondor, and G. Csányi, Phys. Rev. B **87**, 184115 (2013).

[45] Q. Wei, W. Tong, R. Yang, H. Yan, B. Wei, M. Zhang, X. Yang, and R. Zhang, Phys. Lett. A **383**, 125861 (2019).

[46] N. Artrith and A. Urban, Comput. Mater. Sci. **114**, 135 (2016).

[47] S. Lu, Q. Zhou, Y. Ouyang, Y. Guo, Q. Li, and J. Wang, Nat. Commun. **9**, 3405 (2018).

[48] A. Masago, K. Shirai, and H. Katayama-Yoshida, Phys. Rev. B **73**, 104102 (2006).

[49] B. F. Decker and J. S. Kasper, Acta Cryst. **12**, 503 (1959).

[50] E. Yu Zarechnaya, L. Dubrovinsky, N. Dubrovinskaia, N. Miyajima, Y. Filinchuk, D. Chernyshov, and V. Dmitriev, Sci. Technol. Adv. Mater. **9**, 044209 (2009).

[51] T. Ogitsu, E. Schwegler, and G. Galli, Chem. Rev. **113**, 3425 (2013).

[52] I. Chuvashova, E. Bykova, M. Bykov, V. Prakapenka, K. Glazyrin, M. Mezouar, L. Dubrovinsky, and N. Dubrovinskaia, Phys. Rev. B **95**, 180102(R) (2017).

[53] See Supplemental Material at http://link.aps.org/supplemental/10.1103/PhysRevB.103.024505 for computational details. Phonon dispersion curves, molecular dynamics, and the crystal structural information of c-B_{24}.

[54] G. Kresse and J. Furthmüller, Phys. Rev. B **54**, 11169 (1996).

[55] G. Kresse and D. Joubert, Phys. Rev. B **59**, 1758 (1999).

[56] P. E. Blöchl, Phys. Rev. B **50**, 17953 (1994).

[57] H. J. Monkhorst and J. D. Pack, Phys. Rev. B **13**, 5188 (1976).

[58] K. Parlinski, Z. Q. Li, and Y. Kawazoe, Phys. Rev. Lett. **78**, 4063 (1997).

[59] A. Togo, F. Oba, and I. Tanaka, Phys. Rev. B **78**, 134106 (2008).

[60] G. J. Martyna, M. L. Klein, and M. Tuckerman, J. Chem. Phys. **97**, 2635 (1992).

[61] P. Giannozzi, S. Baroni, N. Bonini, M. Calandra, R. Car, C. Cavazzoni, D. Ceresoli, G. L. Chiarotti, M. Cococcioni, I. Dabo, A. Dal Corso, S. de Gironcoli, S. Fabris, G. Fratesi, R. Gebauer, U. Gerstmann, C. Gougoussis, A. Kokalj, M. Lazzeri, L. Martin-Samos, N. Marzari, F. Mauri, R. Mazzarello, S. Paolini, A. Pasquarello, L. Paulatto, C. Sbraccia, S. Scandolo, G. Sclauzero, A. P. Seitsonen, A. Smogunov, P. Umari, and R. M. Wentzcovitch, J. Phys.: Condens. Matter **21**, 395502 (2009).

[62] J. Etourneau, J.-P. Mercurio, and P. Hagenmuller, in *Boron Refract Borides*, edited by V. I. Matkovich (Springer, Berlin, 1977), pp. 115–138.
[63] I. Popov, N. Baadji, and S. Sanvito, Phys. Rev. Lett. **108**, 107205 (2012).
[64] J. Etourneau and P. Hagenmuller, Philos. Mag. Part B **52**, 589 (1985).
[65] X. Li, X. Huang, D. Duan, G. Wu, M. Liu, Q. Zhuang, S. Wei, Y. Huang, F. Li, Q. Zhou, B. Liu, and T. Cui, RSC Adv. **6**, 18077 (2016).
[66] T. Chen, Q. Gu, Q. Chen, X. Wang, C. J. Pickard, R. J. Needs, D. Xing, and J. Sun, Phys. Rev. B **101**, 054518 (2020).
[67] X. Sun, X. Liu, J. Yin, J. Yu, Y. Li, Y. Hang, X. Zhou, M. Yu, J. Li, G. Tai, and W. Guo, Adv. Funct. Mater. **27**, 1603300 (2017).
[68] D. Y. Zubarev and A. I. Boldyrev, Phys. Chem. Chem. Phys. **10**, 5207 (2008).
[69] T. R. Galeev, B. D. Dunnington, J. R. Schmidt, and A. I. Boldyrev, Phys. Chem. Chem. Phys. **15**, 5022 (2013).
[70] H. Zhang, Y. Li, J. Hou, A. Du, and Z. Chen, Nano Lett. **16**, 6124 (2016).
[71] H. Wang and Q. An, J. Phys. Chem. C **123**, 12505 (2019).
[72] Y. Gao, Y. Xie, Y. Chen, J. Gu, and Z. Chen, Phys. Chem. Chem. Phys. **20**, 23500 (2018).
[73] Z. Zhao, F. Tian, X. Dong, Q. Li, Q. Wang, H. Wang, X. Zhong, B. Xu, D. Yu, J. He, H.-T. Wang, Y. Ma, and Y. Tian, J. Am. Chem. Soc. **134**, 12362 (2012).
[74] W. L. McMillan, Phys. Rev. **167**, 331 (1968).
[75] P. B. Allen and R. C. Dynes, Phys. Rev. B **12**, 905 (1975).
[76] J. P. Carbotte, Rev. Mod. Phys. **62**, 1027 (1990).
[77] L. N. Oliveira, E. K. U. Gross, and W. Kohn, Phys. Rev. Lett. **60**, 2430 (1988).
[78] M. I. Eremets, V. V Struzhkin, H. Mao, and R. J. Hemley, Science **293**, 272 (2001).
[79] M. Gao, Q.-Z. Li, X.-W. Yan, and J. Wang, Phys. Rev. B **95**, 024505 (2017).
[80] Y. Ma, J. S. Tse, D. D. Klug, and R. Ahuja, Phys. Rev. B **70**, 214107 (2004).
[81] H. J. Xiang, Z. Li, J. Yang, J. G. Hou, and Q. Zhu, Phys. Rev. B **70**, 212504 (2004).
[82] H. J. Choi, D. Roundy, H. Sun, M. L. Cohen, and S. G. Louie, Phys. Rev. B **66**, 020513(R) (2002).
[83] Z. Zhao, S. Zhang, T. Yu, H. Xu, A. Bergara, and G. Yang, Phys. Rev. Lett. **122**, 097002 (2019).
[84] A. P. Drozdov, M. I. Eremets, I. A. Troyan, V. Ksenofontov, and S. I. Shylin, Nature (London) **525**, 73 (2015).
[85] X. Zhong, H. Wang, J. Zhang, H. Liu, S. Zhang, H.-F. Song, G. Yang, L. Zhang, and Y. Ma, Phys. Rev. Lett. **116**, 057002 (2016).
[86] M. Iuga, G. Steinle-Neumann, and J. Meinhardt, Eur. Phys. J. B **58**, 127 (2007).
[87] X.-Q. Chen, H. Niu, D. Li, and Y. Li, Intermetallics **19**, 1275 (2011).
[88] Z. J. Wu, E. J. Zhao, H. P. Xiang, X. F. Hao, X. J. Liu, and J. Meng, Phys. Rev. B **76**, 054115 (2007).
[89] Q. Li, H. Liu, D. Zhou, W. Zheng, Z. Wu, and Y. Ma, Phys. Chem. Chem. Phys. **14**, 13081 (2012).
[90] V. L. Solozhenko, O. O. Kurakevych, and A. R. Oganov, J. Superhard. Mater. **30**, 428 (2008).